

Effect of pre-deformation of rolling combined with stretching on stress corrosion of aluminum alloy 2519A plate

ZHANG Xin-ming, LIU Ling, YE Ling-ying, LIU Jun, LEI Zhao, SONG Ji-chao

School of Materials Science and Engineering, Central South University, Changsha 410083, China

Received 22 December 2010; accepted 4 April 2011

Abstract: The effect of the pre-deformation of rolling combined with stretching on the stress corrosion cracking resistance of aluminum alloy 2519A was studied by means of the slow strain rate technique at 10^{-6} s^{-1} . The tensile strength and stress corrosion index of the alloy plate with 7% rolling plus 3% perpendicular stretching were 481 MPa and 0.0429, respectively, showing better mechanical property and stress corrosion cracking resistance than those with 4% rolling plus 3% parallel stretching or 7% rolling plus 3% parallel stretching, which is due to its finer and denser precipitates within the grains, discontinuous grain boundary precipitates, as well as more narrow precipitate-free zone width. Such microstructure is attributing to the denser and more homogeneously distributed dislocations which are produced by the pre-deformation.

Key words: 2519A aluminum alloy plate; stress corrosion cracking; pre-deformation; precipitates

1 Introduction

The aluminum alloy 2519, which has a good combination of mechanical properties, weldability, acceptable ballistic resistance and SCC (stress corrosion cracking) resistance, is an Al–Cu–Mg alloy with high Cu/Mg ratio. It has been used for advanced amphibious assault vehicles [1, 2]. By improving the element contents of the alloy, a new version armor alloy as 2519A alloy with higher mechanical properties and SCC resistance was obtained [3, 4].

As the anodic solution mechanism of SCC [5, 6], the tendency of intergranular stress corrosion cracking of aluminum alloy can be controlled by suppressing the nucleation and growing of the precipitates on the grain boundaries [7]. For 2xxx aluminum alloy, pre-deformation is an effective way to control the precipitates on the grain boundaries [8, 9]. The effect of the pre-deformation on the resistance to stress corrosion of 2519A aluminum alloy plate has been investigated, and the alloy with the T8 temper (adding pre-deformation prior to aging) has less stress corrosion susceptibility than that with the T6 temper [10]. On the other hand, the co-plane slip attributed to the coarseness of the θ' phase that results in the glide step increasing

and crack tip can also be suppressed by the pre-deformation for the fine and dispersed precipitates in the alloy plates [10].

Researchers [11–13] have focused on the effect of pre-reduction on the mechanical properties or corrosion resistance of the aluminum alloy 2519A to obtain a preferable pre-deformation range on account of the positive effect of the pre-deformation on the microstructure of 2519A aluminum alloy. Most of them paid attention to the pre-deformation degree on the effect of stress corrosion resistance. However, DYMEK and DOLLAR [14] studied the effect of the pre-deformation mode on the resistance to SCC in aluminum alloy 2519. It was found that the pre-deformation comprising both cold-rolling and stretching prior to aging was more beneficial to SCC resistance than stretching alone, since it produced a more homogeneous dislocation substructure which provided more uniformly distributed potential nucleation sites for the hardening precipitates. The effect of the dislocation distribution on the morphology and dispersion of the second phases had been mentioned [15, 16], indicating that the second phase will coarsen around the dislocation tangle or in the dislocation cell wall. According to FERNANDES and VIEIRA [17] and SCHMITT et al [18], in a complex deformation mode (rolling plus stretching), the dislocation

tangles or dislocation cells produced by the first deformation will come to be dispersed in the initial stage of the second deformation. The aim of this work is to investigate how the precipitation will be influenced by different dislocations due to different complex pre-deformation modes and then affect the SCC of the 2519A alloy plate. The proper candidate pre-deformation mode which can promote the SCC resistance of the alloy plate will be explored by employing three different kinds of complex pre-deformation modes.

2 Experimental

Hot-rolled 2519A aluminum plate with thickness of 6 mm and the chemical compositions of (in mass fraction, %) 5.80 Cu, 0.20 Mg, 0.29 Mn and 0.20 Zr was further hot-rolled to final thickness of 2 mm. The alloy plates were subjected to a solution-treatment at 533 °C followed by pre-deformation and subsequently aged at 165 °C. Table 1 shows the pre-deformation of alloy plate A, alloy plate B, and alloy plate C. The stress corrosion cracking tests of the peak-aged alloy plates after pre-deformation were carried out in a solution of 3.5% NaCl in the long transverse direction by using the slow-strain-rate technique (SSRT). Specimens were tested in the WDM-3 tensile machine with a load of 30 kN. The tests were carried out by triplicate at strain rate of 10^{-6} s^{-1} . Dry control tests were also carried out at the same strain rate in order to evaluate the comparative ductility loss, fracture energy loss and stress corrosion index.

Table 1 Pre-deformation mode for alloy plates

Alloy plate	Pre-deformation mode
A	Rolling 4%+// stretching 3%
B	Rolling 7%+// stretching 3%
C	Rolling 7%+⊥ stretching 3%

TEM observations were made in bright field imaging modes on TecnaiG²20 microscope operating at 200 kV to study the microstructure. The disk specimens for TEM were taken from the top side of the plate, prepared by twin-jet electro-polishing in a solution of 30% HNO₃-methanol at -15 V and -25 °C cooled by liquid nitrogen.

In order to analyze the corrosion resistance of the alloy plates in the corrosion environment, the electrochemical behavior was studied by Tafel polarization curve gained by zeta potential scanning method in 3.5% NaCl. The test was carried out in the CHI660C electrochemical workstation at 25 °C in a three-electrode structure with platinum electrode being the counter electrode and SCE(saturated calomel electrode) being the reference electrode. The scanning

voltage was from -1.0 V to -0.2 V and the scan rate was 0.002 V/s. The samples were grinded by waterproof abrasive paper, cleaned by alcohol and acetone, and then sealed by wax and colophony with a proportion of 1:1, except leaving a test surface with unite area. Grain shape of the plates in longitudinal section was analyzed by the optical microscopy.

3 Results and discussion

3.1 Stress corrosion test

By hardness test, the peak-aging time of alloy plates A, B and C was 15 h, 12 h and 12 h determined, respectively. Figures 1 and 2 show the stress—strain curves tested in air and in 3.5% NaCl solution for the three different pre-deformed alloy plates after peak-aging. The tensile strength, elongation, fracture energy corresponding to each alloy plate are illustrated in Table 2. The fracture energy was obtained by the area integral of the stress—strain curve. It is evident that alloy plate C has the highest aging strength, fracture energy and the best elongation tested either in air or in 3.5% NaCl. The

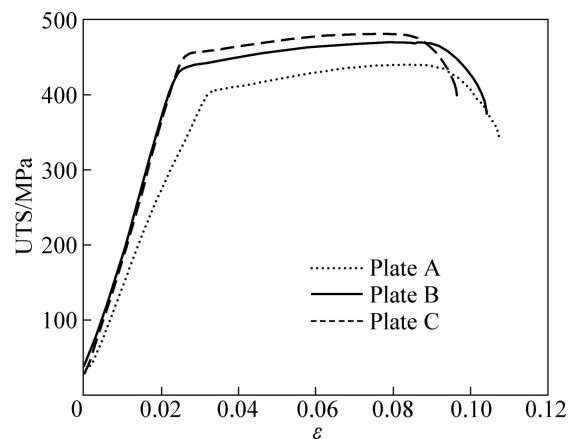


Fig. 1 Stress—strain curves of alloy plates peak-aged at 165 °C and stretched in air (strain rate: 10^{-6} s^{-1})

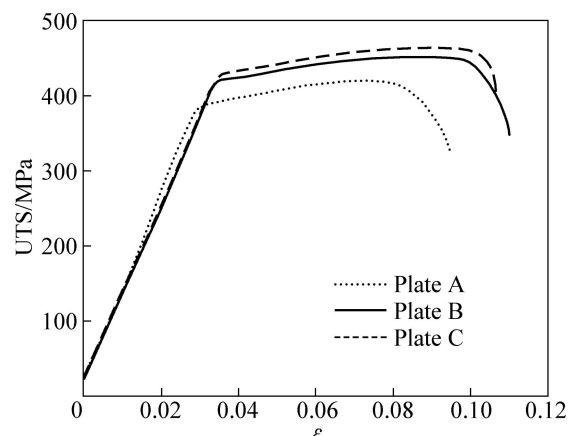


Fig. 2 Stress—strain curves of alloy plates peak-aged at 165 °C and tensed in 3.5% NaCl (strain rate: 10^{-6} s^{-1})

relative value of the tensile strength loss and fracture energy loss, as well as stress corrosion index I_{SSRT} , which are exhibited in Table 3, were gained from Table 2, where the stress corrosion index I_{SSRT} is given by

$$I_{SSRT} = 1 - \frac{\sigma_{fw}(1 + \delta_{fw})}{\sigma_{fA}(1 + \delta_{fA})} \quad (1)$$

where σ_{fw} and δ_{fw} are the tensile strength and elongation gained from tests in 3.5% NaCl, respectively; σ_{fA} and δ_{fA} are the tensile strength and elongation gained from tests in air, respectively [19]. It is explicitly observed that alloy plate C shows the best stress corrosion resistance, since it presents the lowest I_{SSRT} and fracture energy, as well as little loss of tensile strength.

Table 2 Tensile strength, elongation, fracture energy values of three pre-deformed alloy plates peak-aged at 165 °C, tested in air and in 3.5% NaCl solution, respectively

Alloy plate	Medium	Tensile strength/MPa	Elongation/%	Fracture energy/(J·cm ⁻³)
A	Air	439	9.2	38.8
	3.5% NaCl	421	7.9	32.3
B	Air	468	9.1	41.8
	3.5% NaCl	452	8.6	35.8
C	Air	481	9.0	41.9
	3.5% NaCl	465	8.8	40.1

Table 3 Stress corrosion index, tensile strength loss and fracture energy loss of plates tested in 3.5% NaCl solution compared with those of plates tested in air

Alloy plate	Tensile strength loss/%	Fracture energy loss/%	Stress corrosion index
A	4.1	16.8	0.1632
B	3.4	14.4	0.0820
C	3.3	4.3	0.0429

3.2 Microstructure

Precipitation microstructure is the main factor that influences the SCC resistance of the alloy plates and it may be affected by the dislocation distribution produced ascribing to the pre-deformation mode. High densities of dislocations are clearly visible within the grains of all the alloy plates, as shown in Fig. 3. Figures 3 shows the images of dislocations of alloy plates A, B and C, respectively. Owing to greater pre-deformation, alloy plates B and C have higher dislocation density than plate A. However, the dislocation of alloy plate C is not only denser, but also more homogeneous than plate B. During the 4% rolling reduction in alloy plate A, the dislocation slip just started and the dislocation density was low. But the 7% rolling reduction in alloy plates B and C generated more mobile dislocations which became dense

after the following 3% stretching, even though the dislocation multiplication was not easy in such a low stretching. In alloy plate C, the direction of the following stretching changed. It made the tangled dislocations come to be dispersed and some new dislocation slip systems activated. Thereby, the higher density and more equally distributed dislocations were attained in alloy plate C.

2519A alloy is a typical age-hardenable alloy which is strengthened by the semi-coherent fine θ' phase (Al_2Cu) precipitate. Figure 4 displays the TEM images within the

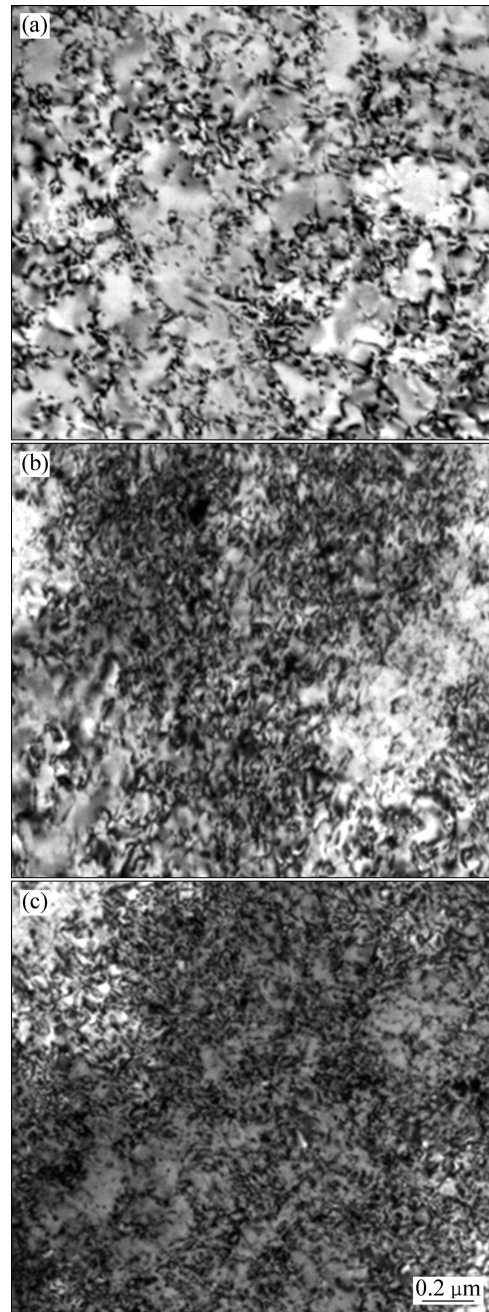


Fig. 3 TEM bright field images showing dislocations of pre-deformed alloy plates prior to aging: (a) Alloy plate A; (b) Alloy plate B; (c) Alloy plate C

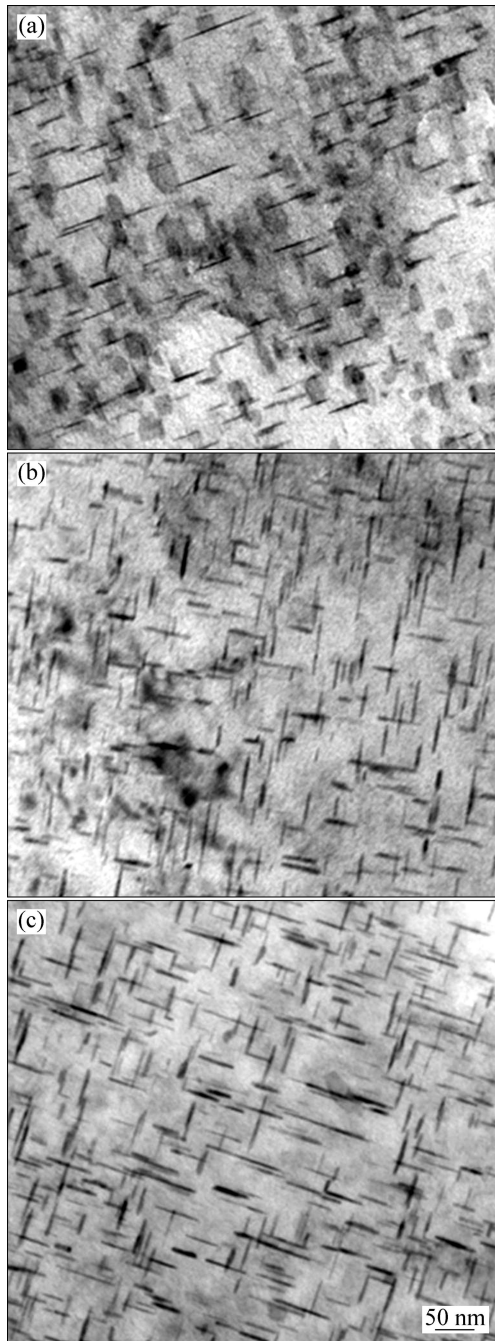


Fig. 4 TEM bright field images showing θ' phases within grains from pre-deformation alloy plates peak-aged at 165 °C: (a) Alloy plate A; (b) Alloy plate B; (c) Alloy plate C

grains from the three different pre-deformed alloy plates peak-aged at 165 °C. The precipitates within the grains in alloy plates B and C are denser than those in alloy plate A. This denser precipitates are accordant with the higher density dislocations which were demonstrated by Figs. 3(b) and Fig. 3(c). The dislocations can provide efficient sites for the heterogeneous nucleation of the precipitates and fast diffusion paths for the solute atoms during aging. The higher density dislocations can supply

more nucleation sites for the precipitations. However, the distribution of the precipitates within the grains in alloy plate C is more homogeneous than that in alloy plate B. It is due to its more homogeneous distribution dislocations, as discussed above. So, the distribution of the dislocations can influence the distribution of the precipitates, and the homogeneous distribution precipitates are more beneficial to the mechanical property of the alloy plate.

The TEM images of the grain boundaries in the three different pre-deformed alloy plates peak-aged at 165 °C are presented in Fig. 5, which are the statistics of the PFZ (precipitate-free zone) width and precipitate size in Table 4. The grain boundary precipitates (GBP) of alloy plate C are not only finer, but also have discontinuous distribution. What is more, the PFZ width in alloy plate C is lower. As the anodic solution mechanism of the intergranular corrosion, a corrosion cell can form between the GBP and the PFZ on account of their potential difference. The cathode of the GBP is rich of element Cu, showing higher electric potential, while the anode of the PFZ is lack of element Cu, showing lower electric potential [20]. The potentials of θ (θ') phase, PFZ and matrix were -0.53 , -0.78 and -0.68 V, respectively [14]. The reduction of the GBP decreases the potential difference between the cathode and the anode, making the intergranular corrosion not easy to happen. And the discontinuous GBP prevents the forming of a continuous passage of the intergranular corrosion [11]. On the other hand, the comparison between the electric potential of the PFZ near the grain boundary and the electric potential inner grain shows that the former was generally lower than the latter. This potential difference can lead to another corrosion cell forming, and the PFZ near the grain boundary will be first dissolved once the corrosion happens. Then in the effect of stress, the microcrack will take place, develop along the corrosion passage and lead to the intercrystalline cracking ultimately.

Table 4 Statistics of precipitation size in grain boundaries in different pre-deformed alloy plates peak-aged at 165 °C

Alloy plate	PFZ width/nm	Diameter of second phase/nm
A	140.0	191.0
B	90.0	90.7
C	75.0	49.4

At the same time, the fine and disperse precipitates within the grains not only decrease the glide steps and crack tip on the alloy surface which may aggravate the happening of SCC [10], but also are beneficial to the homogeneous distribution of the electric potential in the

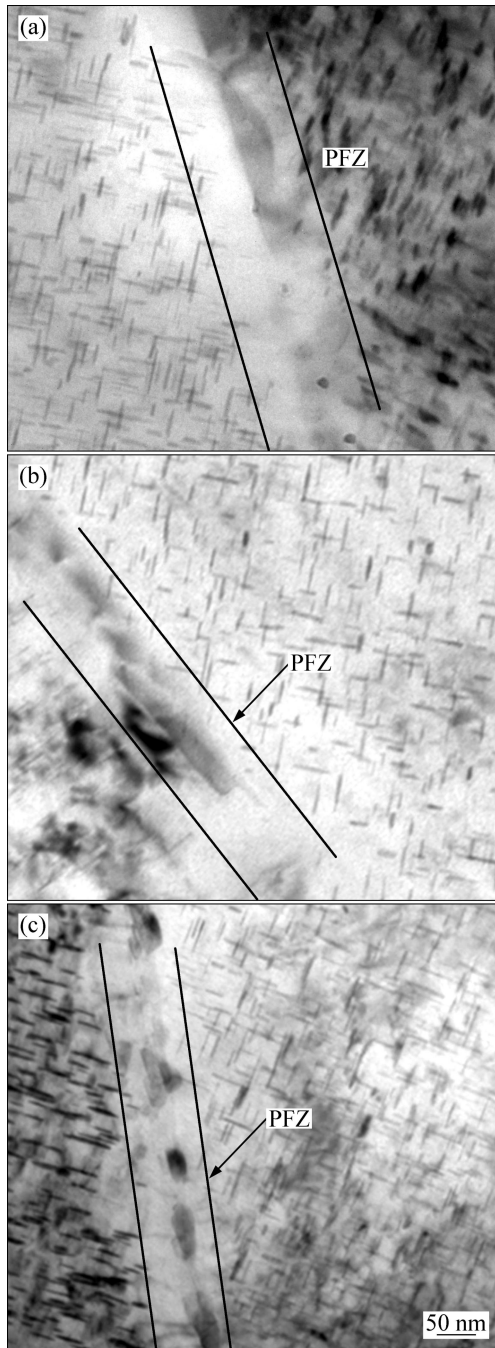


Fig. 5 TEM bright field images showing θ' phases in grain boundary in three kinds of pre-deformation alloy plates peak-aged at 165 °C: (a) Alloy plate A; (b) Alloy plate B; (c) Alloy plate C

grains, which can reduce the local corrosive pitting around the places with high electric potential, such as the coarse precipitates. The susceptibility of aluminum alloys to localized corrosion strongly depends on the distribution and electrochemical properties of second phase particles. According to the rupture of brittle passive film theory [19], the oxidation film of the corrosion pit will slip along with the metal matrix in the effect of stress and then crack, exposing the new metal

surface. The electric potential of the new metal surface is lower than its surrounding environment, making it much easier to be eroded. Moreover, the anodic area of the new alloy surface is much smaller than the surrounding cathodic area, which accelerates its eroding rate. Therefore, a corrosion pit could develop constantly, penetrate deeply, and finally lead to the transgranular or intergranular fracture with stress.

3.3 Polarization curves

Mostly, corrosion is the beginning of the SCC procedure in which corrosion resistance is an important factor of SCC resistance of the alloy plates. Figure 6 shows the polarization curves of the three different pre-deformed alloy plates prior to aging and peak-aging. The three curves in Fig. 6(a) show a similar polarization behavior and each of them relates a rapid rising in anodic current density. The three curves in Fig. 6(b) also show a similar polarization behavior, but the rising rate of the

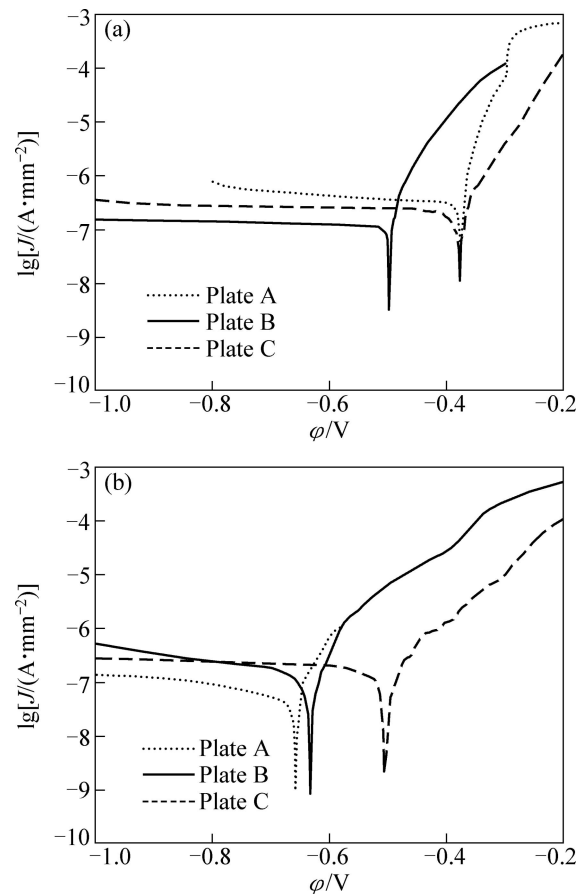


Fig. 6 Polarization curves of three different pre-deformed alloy plates: (a) No-aged alloy; (b) Peak-aged alloy (The tests were processed by zeta potential scanning method in 3.5% NaCl at 25 °C in a three-electrode structure with platinum electrode being counter electrode and SCE (saturated calomel electrode) being reference electrode. The scanning voltage was from -1.0 V to -0.2 V and the scan rate was 0.002 V/s)

anodic current density in each curve obviously descends compared with that in Fig. 6(a). The onset of pitting is not observed visibly in Fig. 6(b), which means that E_{pit} is very close to φ_{corr} [20, 21], because pitting is the main corrosion way when the alloy plate is soaked in 3.5% NaCl solution.

Table 5 shows the corresponding φ_{corr} and corrosion current density (J) obtained from these curves. The φ_{corr} is the abscissa value of the intersection between the anodic polarization curve and the cathodic polarization curve. The corrosion current density was gained by making tangents over both the anodic and the cathodic polarization curve. Then the ordinate value of the intersection point of the two tangents is the value of the corrosion current density. The order of corrosion current density of all the three alloy plates prior to aging is 10^{-7} , decreases to 10^{-8} after peak-aging, but exhibits little difference between each other. However, the difference of φ_{corr} cannot be ignored. Before aging, as the defects within the grains increased with deformation, the φ_{corr} of alloy plate B was more negative than that of alloy plate A, while alloy plate C was not. After peak-aging, the φ_{corr} of all the alloy plates became negative, and the difference between each other was also obvious. The φ_{corr} values of the three alloy plates from negative to positive are: φ_{corr} of alloy plate A < φ_{corr} of alloy plate B < φ_{corr} of alloy plate C. This is well coincident with the SSRT test result.

Table 5 φ_{corr} and corrosion current density J of three different pre-deformed alloy plates no-aged and peak-aged at 165 °C

Alloy plate	Treatment	$\varphi_{\text{corr}}/\text{V}$	$J/(\text{A}\cdot\text{mm}^{-2})$
A	No-aged	-0.376	7.6×10^{-7}
	Peak-aged at 165 °C for 15 h	-0.658	5.5×10^{-8}
B	No-aged	-0.499	1.8×10^{-7}
	Peak-aged at 165 °C for 12 h	-0.634	7.7×10^{-8}
C	No-aged	-0.378	1.7×10^{-7}
	Peak-aged at 165 °C for 12 h	-0.507	6.9×10^{-8}

The φ_{corr} difference of the alloy plates prior to aging is related to the pre-deformation degree and pre-deformation mode. Compared with alloy plate A, alloy plate B had more grain defects for more deformation, and the electrochemical inhomogeneity was also more serious, either inside an individual grain or between each grain. Defects which were active places in electrochemical corrosion could lead to the decrease of φ_{corr} . Whereas, the φ_{corr} of alloy plate C remained unchanged after more deformation. This may be responsible to its different grain shapes. As shown in

Fig. 7, the grain shape of alloy plate C which is near to isoaxial after stretching along stretching direction perpendicular to rolling direction is different from the long strip grain shape of alloy plates A or B stretched along stretching direction parallel to rolling direction. The equiaxial grains were the result of homogeneous deformation between the transverse and longitudinal direction, which exhibited more electrochemical homogeneity than the long strip grains. The deformation homogeneity has also been discussed above in the TEM image of the dislocations.

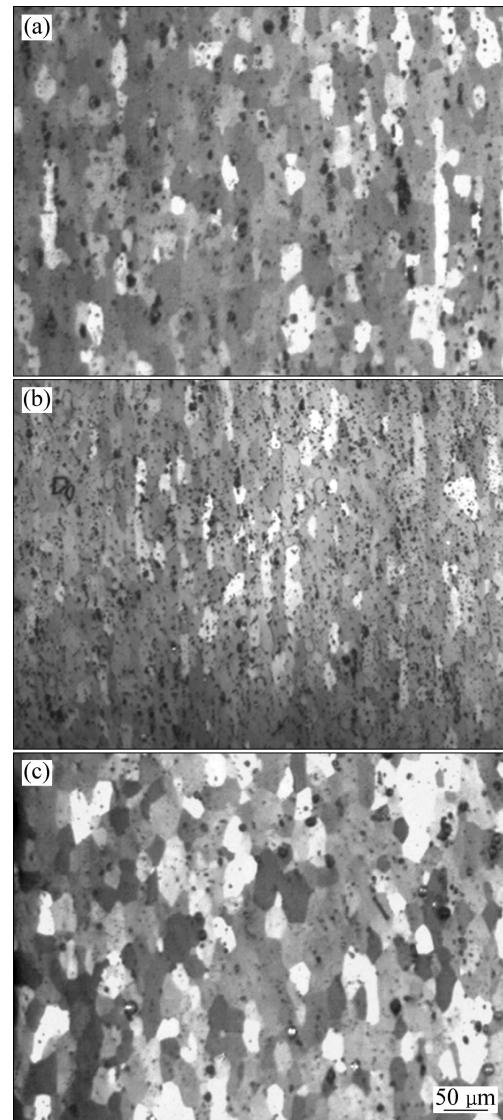


Fig. 7 Grain structure in different pre-deformed alloy plates prior to aging: (a) Alloy plate A; (b) Alloy plate B; (c) Alloy plate C

As the analysis above, it is the precipitates in the grains and the grain boundaries that cause the difference of φ_{corr} and SCC resistance of the three alloy plates peak-aged. But the shape of the grains is also an important factor which should be considered. With the

susceptibility to intergranular corrosion of the alloy plates, the cracks tend to grow along pre-existing paths, and grain boundaries. In the report of stress corrosion cracking behavior of the 8090 Al-Li alloy, CONDE and DAMBORENEA [6] suggested that the crack had to change its orientation when passing from one grain to another during its growth. An elongated grain can hinder the crack growing perpendicularly to the stress, making it grow parallel to the stress and the stress acting at the tip is lower with attenuated growth rate. In this study, the influence of the precipitations on anodic dissolution is the predominant factor for the SCC resistance, while the elongated grain shape may also delay the crack growth progress.

4 Conclusions

1) Compared with 4% rolling plus 3% parallel stretching and 7% rolling plus 3% parallel stretching, the tensile strength and stress corrosion index of the alloy plate with 7% rolling plus 3% perpendicular stretching were 481 MPa and 0.0429, showing the best mechanical property and SCC resistance.

2) The 7% rolling plus 3% perpendicular stretching produced not only high but also homogeneous distributed dislocations, which made the precipitates within grains not only denser, but also distribute more homogeneously, and the GBP size and PFZ width were also smaller than the other alloy plates. The dispersion of dislocations and precipitates is not only related to the complex pre-deformation degree, but also is affected by the deformation path of rolling and stretching.

References

- [1] JAMES J, FISHER J. Aluminum alloy 2519 in military vehicles [J]. *Advanced Materials and Processes*, 2002, 160(9): 43–46.
- [2] HAMILTON B C, SAXENA A. Transient crack growth behavior in aluminum alloys C415-T87 and 2519-T87 [J]. *Engineering Fracture Mechanics*, 1999, 62(1): 1–22.
- [3] GAO Zhi-guo, ZHANG Xin-ming, CHEN Min-an. Investigation on θ' precipitate thickening in 2519A-T87 aluminum alloy plate impacted [J]. *Journal of Alloys Compound*, 2009, 476(1–2): 1–3.
- [4] LI Hui-zhong, ZHANG Xin-ming, CHEN Min-an, LIU Ying, ZHOU Zhuo-ping. Effect of Cu on microstructure and mechanical properties of 2519 aluminum alloy [J]. *Transactions Nonferrous Metals Society of China*, 2005, 15(5): 1026–1030.
- [5] CHANG C H, LEE S L, LIN J C, YEH M S, JENG R R. Effect of Ag content and heat treatment on the stress corrosion cracking of Al-4.6Cu-0.3Mg alloy [J]. *Materials Chemistry and Physics*, 2005, 91(4): 454–462.
- [6] CONDE A, de DAMBORENEA J J. Stress corrosion cracking behavior of 8090 Al-Li alloy at 313 K. The effect of grain structure [J]. *Corrosion Science*, 1999, 41(6): 1079–1088.
- [7] WANG D, MA Z Y. Effect of pre-strain on microstructure and stress corrosion cracking of over-aged 7050 aluminum alloy [J]. *Journal Alloys and Compounds*, 2009, 469(1–2): 445–450.
- [8] GONG Hong-bin, LI Ren-shun. Effect of deformation and recrystallization on stress corrosion cracking susceptibility of 2091 Al-Li alloy [J]. *Scripta Metallurgica et Materialia*, 1994, 31(10): 1431–1436.
- [9] CHEN Xian-feng, PENG Da-shu, ZHANG Hui, LIN Qi-quan, LIN Gao-yong. Influence of heat treatment on mechanical properties and stress corrosion sensitivity of 2519 aluminum alloy plate [J]. *The Chinese Journal of Nonferrous Metals*, 2003, 13(4): 934–938. (in Chinese)
- [10] LI Hui-zhong, ZHANG Xin-ming, CHEN Min-an, LI Yan-fang, LIANG Xiao-peng. Effect of pre-deformation on the stress corrosion cracking susceptibility of aluminum alloy 2519 [J]. *Rare Metals*, 2007, 26(4): 385–390. (in Chinese)
- [11] LIU Ying, ZHANG Xin-ming, LIU Bo, LI Hui-zhong, GAO Hui. Effect of pre-rolling reduction on intergranular corrosion of aluminum alloy 2519A [J]. *Materials Science Forum*, 2007, 546: 1117–1122.
- [12] LIU Ying, ZHANG Xin-ming, LIU Bo, LI Hui-zhong, GAO Hui. Effect of degree of pre-deformation on intergranular corrosion resistance of 2519 aluminum alloy [J]. *The Chinese Journal of Nonferrous Metals*, 2006, 16(9): 1545–1550. (in Chinese)
- [13] LIU Ying, ZHANG Xin-ming, ZHOU Gu-xin, LIU Bo, LI Hui-zhong, GAO Hui, LI Hui-jie. Effect of degree of pre-deformation on exfoliation corrosion resistance of 2519 alloy aluminum alloy [J]. *Transactions of Materials and Heat Treatment*, 2006, 27(6): 61–65. (in Chinese)
- [14] DYMEK S, DOLLAR M. TEM investigation of age-hardenable Al 2519 alloy subjected to stress corrosion cracking tests [J]. *Materials Chemistry and Physics*, 2003, 81(2–3): 286–288.
- [15] LI Ren-shun, CHEN Xiang-ping, WANG Zuo-yi. Effect of pre-rolling deformation on stress corrosion cracking susceptibility of 2091 alloy [J]. *Journal of Astronautics*, 1994, 15(4): 46–51. (in Chinese)
- [16] KRISHNA B V, JANAKI R G D. Tailoring the precipitation in Al alloys through local plastic deformation [J]. *Materials and Design*, 2007, 28(7): 2239–2243.
- [17] FERNANDES J V, VIEIRA M F. Strain distribution in copper tensile specimens pre-strained in rolling [J]. *Metallurgical and Materials Transactions A*, 1997, 28(5): 1169–1179.
- [18] SCHMITT J H, FERNANDES J V, GRACIO J J, VIEIRA M F. Plastic behavior of copper sheets during sequential tension tests [J]. *Materials Science and Engineering A*, 1991, 147(2): 143–154.
- [19] LIU Ji-hua, LI Di, LIU Pei-ying, GUO Bao-lan, ZHU Guo-wei. Effect of ageing and retrogression treatments on mechanical and corrosion properties of 7075 aluminum alloy [J]. *Transactions of Materials and Heat Treatment*, 2002, 23(1): 50–53. (in Chinese)
- [20] HU J, XU L X, YAO C K. Location corrosion of alumina borate whisker reinforced AA2024 T6 composite in aqueous 3.5% NaCl solution [J]. *Materials Chemistry and Physics*, 2002, 76(3): 290–294.
- [21] BURLEIGH T D. The postulated mechanisms for stress corrosion cracking of aluminum alloys [J]. *Corrosion*, 1991, 47(2): 89–98.

冷轧与拉伸复合预变形对 2519A 铝合金板材应力腐蚀的影响

张新明, 刘玲, 叶凌英, 刘军, 雷钊, 宋继超

中南大学 材料科学与工程学院, 长沙 410083

摘 要: 采用 10^{-6} s^{-1} 慢应变拉伸测试手段研究冷轧与拉伸复合预变形对 2519A 铝合金抗应力腐蚀开裂性能的影响。冷轧 7%后再垂直拉伸 3%的合金板材抗拉强度和应力腐蚀指数分别为 481 MPa 和 0.0429, 与冷轧 4%后再平行拉伸 3%以及冷轧 7%后再平行拉伸 3%的合金板材相比表现出了更好的力学性能和抗应力腐蚀开裂性能。这主要是由于冷轧 7%后再垂直拉伸 3%在合金板材中生成了密度更高且分布更均匀的位错组织, 使时效后合金板材晶内析出相细小、密集, 晶界析出相不连续, 晶界无沉淀析出带且较窄。

关键词: 2519A 铝合金板材; 应力腐蚀开裂; 预变形; 析出相

(Edited by YANG Hua)